INTERNATIONAL JOURNAL OF HYDROGEN ENERGY 41 (2016) 17526–17538

Available online at www.sciencedirect.com

ScienceDirect

journal homepage: www.elsevier.com/locate/he

Flatness-based feedforward control of polymer electrolyte membrane fuel cell gas conditioning system

János Kancsár[*], *Martin Kozek*, *Stefan Jakubek*

Institute of Mechanics and Mechatronics, Division of Control and Process Automation, Vienna University of Technology, Austria

ARTICLE INFO

Article history:
Received 17 March 2016
Received in revised form
27 May 2016
Accepted 7 June 2016
Available online 25 July 2016

Keywords:
PEM fuel cell testbed
Nonlinear control
Exact linearisation
Differential flatness

ABSTRACT

Manufacturers of automotive applications rely on high-performance testing environments for the development of polymer electrolyte membrane fuel cell (PEMFC) technologies. The main component of a PEMFC testbed is the gas conditioning system, which controls the inlet gas temperature, stack pressure, relative humidity and mass flow of the gas at the inlet of the PEMFC stack. This paper presents a control concept for a highly dynamic PEMFC gas conditioning system. The main control challenge lies in the decoupling of the governing thermodynamic quantities. Therefore, the nonlinear control concept of exact input–output linearisation with an extended PID control structure is applied. Constraints on the actuators are incorporated by formulating the resulting control law as an optimisation problem. The robustness with respect to parameter uncertainties for the model is shown by investigating the trajectory tracking error of the disturbed system. Simulation results show an overall good performance for the trajectory tracking and demonstrate the robustness of the model against parameter uncertainties.

Introduction

Due to increasing emission standards [1], automotive manufacturers are looking for ways to reduce pollution or even replace internal combustion engines by alternative propulsion systems. One of the most promising technologies are polymer electrolyte membrane fuel cell (PEMFC) powered vehicles. Compared to other fuel cell technologies, PEMFCs have the advantages of operating at low temperature, fast response, high power density and zero emission.

By utilising the electrochemical reaction of hydrogen and oxygen to create energy, the emission of air pollutants is decreased to zero. In order to develop and increase the efficiency of PEMFC systems, manufacturers rely on a high performance testing environment on component level. A schematic view of a fuel cell system is given in Fig. 1. The gas conditioning system in a PEMFC system is one of the main components, and it is responsible for conditioning the inlet gas for the PEMFC stack.

There are four main control tasks for a PEMFC gas conditioning system. These deduce from the main challenges to reduce the rate of degradation of the PEMFC membrane under load changes [2].

First, the control of the inlet gas mass flow rate. This provides the gas supply for the fuel cell and prevents the system from lack of reactants and, therefore, prevents the stack from so called starvation, which would otherwise increase the degradation of the stack [3,4].

* *Corresponding author*. Tel.: +43 1 58801 325518.
E-mail address: janos.kancsar@tuwien.ac.at (J. Kancsár).
http://dx.doi.org/10.1016/j.ijhydene.2016.06.086
0360-3199/

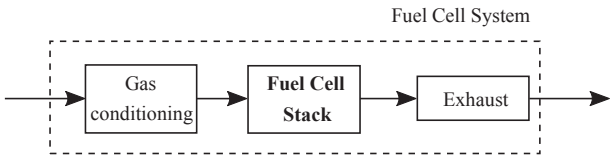

Fig. 1 – Schematic view of a Fuel Cell System.

Second, the control of the stack pressure. The stack pressure is an important quantity for the power output of the fuel cell system. But a large pressure difference between anode and cathode damages the membrane in the fuel cell. Therefore, it is important to regulate the pressure in the fuel cell to prevent the membrane from damage and increase the life time of the fuel cell.

Third, the control of the relative humidity. Water management is one of the most critical issues in the operation of PEMFCs [5–7]. It is most vital to keep the membrane hydrated. Therefore, it is important to control the relative humidity of the supplied gases and prevent the dry out of the membrane under load changes.

Fourth, the control of the gas inlet temperature. Due to the coupling of the temperature to the relative humidity, it is evident to additionally control the gas inlet temperature.

These lead to the control requirements of a gas conditioning system: inlet gas mass flow control, stack pressure control, gas inlet temperature control and control of the relative humidity of the stack. These thermodynamic quantities are coupled through various relations. To successfully control such a system, it is of utmost importance to understand these couplings and to consider them for the design of the controller. Additionally, the application of PEMFCs in automotive applications requires operation under highly dynamic load changes and therefore, a fast and accurate transient response of the control variables.

Much research has been done in the control of PEMFC systems, which also includes the control of the inflowing gases. Most authors deal with the control of the pressure of the gases in the fuel cell system and isolate the flow/pressure dynamics from the temperature and humidity dynamics. In Refs. [8,9], the authors focus on the pressure difference of anode and cathode side. The gas temperature is assumed to be equal to the stack temperature and, therefore, temperature dynamics is not considered. They apply a second order sliding mode controller to control the anode and cathode pressure. In Refs. [10,11], a feedback and feedforward strategy was applied to control the air supply of a PEMFC system. However, the control approach was based on PEMFC models, which were linearised around a specific operating point. The authors considered a fixed cathode air temperature and one control variable and focused on achieving the required system net power after step changes. Although in Refs. [12], the authors state the importance of the effects of humidity and temperature on the fuel cell, they did not consider it further in the modelling, due to limitation in their hardware setup. In Refs. [13,14], the authors focus on the pressure of the gases and did not consider the humidification. They utilise the concept of feedback linearisation to design a controller for their PEMFC model. Additionally, they applied a PI controller to obtain a more robust control. In Refs. [15], the authors focused on the pressure of hydrogen and oxygen. The gas temperature at the inlet was considered to be equal to the stack temperature. The authors applied feedback linearisation and designed an H_∞ controller for their PEMFC model. Their main focus was to avoid pressure fluctuation, which could damage the membrane. In Refs. [16], the authors controlled the cathode pressure and oxygen excess ratio by applying a flatness-based control concept. In Ref. [17] the authors propose a fuzzy-PID control for air flow regulation and analyse and verify the simulation results to prove the efficiency of the proposed fuzzy-PID control against the conventional PID control. They conclude that a feedforward part is a great help to improve the performance. In Ref. [18] the authors investigated a time delay control to increase the transient performance of PEM fuel cells. In Ref. [19] the authors implemented a model predictive control to manipulate the air flow rate entering the fuel cell. Although the fast response time of the system is not required, a partly similar control problem arises in the control of heating, ventilating, and air conditioning (HVAC) systems. In such systems, the main objective is to control the temperature and humidity of the air to create a comfortable ambience. Here it is dealt with the problem of the thermodynamic coupling of temperature and relative humidity. But the mass flow rate of air and the pressure of the ambience are not considered. In Refs. [20,21], the authors applied nonlinear control strategies to HVAC systems and achieved a better control result than with conventional approaches. Overall, the focus in the design of PEMFC controllers lies on the control and decoupling of the pressure on the anode and cathode side and decoupling pressure and mass flow, respectively. Temperature and humidity dynamics are rarely considered. On the other hand, in the design of HVAC systems the dynamics of temperature and humidity are treated, but pressure and mass flow dynamics are not considered.

In this paper, we address both issues and present a control concept for a highly dynamic testing environment for PEMFC stacks, which controls the inlet gas temperature, stack pressure, relative humidity and gas mass flow. This represents a nonlinear control problem with multiple inputs and multiple outputs (MIMO). In order to achieve a better dynamic response, we incorporate the actuator dynamics of the gas conditioning system as first order differential equations. To this coupled set of equations, we apply the method of exact input–output linearisation and decouple the system. To achieve a robust decoupling, we take advantage of the differential flatness of the system. The constraints on the actuators are included by formulating the control law as an optimisation problem. To the resulting decoupled system we apply a feedforward control and a PID control structure to achieve both a good setpoint tracking and good disturbance rejection. By applying Lyapunov's stability theory, we show that the concept is robust against tested parameter uncertainties.

This paper is structured as follows: In Section PEMFC gas conditioning system, the model for the gas conditioning system is presented. In Section Exact linearisation of MIMO nonlinear system, the concept of exact linearisation and differential flatness is introduced and applied to the model of the gas conditioning system. The robustness of the system is investigated in Section Robustness analysis. The simulation results are presented in Section Simulation results. Conclusions are given in Section Conclusion.

PEMFC gas conditioning system

In the following, we present the hardware concept for a gas conditioning system for a PEMFC testbed and derive the mathematical model, which describes the system. For the reason of readability, first, we introduce the subscripts G for gas and S for steam and second, we use the operator $\frac{d}{dt}$ to indicate a time derivative and the dot operator to indicate a mass flow. In the following sections we only use the dot operator because the mass flow is part of the state vector and we do not need to distinguish between time derivatives and mass flows.

Hardware setup for the gas conditioning system

As depicted in Fig. 1, the gas conditioning system for the PEMFC stack takes in gas and provides a controlled environment for the fuel cell stack. It accomplishes this by controlling the inlet gas temperature, stack pressure, relative humidity and gas mass flow to the stack.

In Fig. 2, a schematic of a gas conditioning system for the cathode channel of a PEMFC is shown. Pressurised gas and steam are provided at the testbench. The mass flow of both paths is controlled with a mass flow controller (MFC). The air path has an additional heater, while the steam path has a fixed temperature. Both gases are fed into a mixing chamber, which provides the gas mixture at the outlet. The fuel cell (FC) stack cathode is depicted after the mixing chamber. At the outlet of the fuel cell stack cathode, a backpressure valve is located. The control variables for this setup are the two gas mass flows controlled by the mass flow controllers, the power of the heater and the opening area of the backpressure valve. The outputs to be controlled are located behind the mixing chamber. These are the inlet gas temperature, stack pressure, relative humidity and gas mass flow into the fuel cell stack cathode inlet. A summery and the corresponding operating ranges are given in Table 1. The operating ranges are calculated based on a 10 kW PEMFC stack.

Table 1 – Operating ranges of actuators and output variables.

Actuator	Range	Output	Range
u_G	4–40 kgh^{-1}	$\overline{T}$	20–100 °C
$\dot{Q}$	0–9 kW	$\overline{p}$	1.1–3 bar
u_S	0–30 kgh^{-1}	φ	0–100%
u_{Nozzle}	0–2 cm^2	$\dot{m}_{out}$	0–70 kgh^{-1}

Gas dynamics of gas conditioning system model

The mass balance equations in the mixing chamber are given by Eq. (1). The first equation represents the mass balance for air. The second equation represents the mass balance for the steam in the system. The first terms in the equations are the mass flows into the mixing chamber, and the second terms are the outflowing gases.

$$\begin{aligned}\frac{d}{dt}\overline{m}_G &= \dot{m}_{G,\,in} - \dot{m}_{G,\,out}\\ \frac{d}{dt}\overline{m}_S &= \dot{m}_{S,\,in} - \dot{m}_{S,\,out}\end{aligned} \tag{1}$$

The outflowing mass streams in Eq. (1) are given by

$$\dot{m}_{G,\,out} = \frac{\overline{m}_G}{\overline{m}}\,\dot{m}_{out}, \quad \dot{m}_{S,\,out} = \frac{\overline{m}_S}{\overline{m}}\,\dot{m}_{out} \tag{2}$$

with

$$\overline{m} = \overline{m}_G + \overline{m}_S. \tag{3}$$

The outflowing mass streams of gas and steam are given by the mass fractions of the total mass $\overline{m}$ in the system.

The energy balance of the system is given by Eq. (4).

$$\frac{dU}{dt} = \dot{m}_{G,in}h_{G,in} + \dot{m}_{S,in}h_{S,in} - \dot{m}_{out}h_{out}, \tag{4a}$$

$$\frac{dU}{dt} = \frac{d}{dt}(\overline{m}_G\overline{u}_G + \overline{m}_S\overline{u}_S) \tag{4b}$$

where $h_{G,in}$, $h_{S,in}$ and h_{out} are the specific enthalpies of the gases and are given by Eq. (6) and $\overline{u}_G$ and $\overline{u}_S$ represent the specific internal energy of the gases.

With Eq. (2) the last term in Eq. (4a) can be written as

$$\dot{m}_{out}h_{out} = \frac{1}{\overline{m}}\dot{m}_{out}(\overline{m}_G h_{G,\,out} + \overline{m}_S h_{S,\,out}). \tag{5}$$

The specific enthalpies of the gases are defined as

$$h_{G,\,in} = c_{p,G}T_{G,in}, \quad h_{S,\,in} = c_{p,S}T_{S,in} + r_0, \tag{6a}$$

$$h_{G,\,out} = c_{p,G}\overline{T}, \quad h_{S,\,out} = c_{p,S}\overline{T} + r_0 \tag{6b}$$

where $\overline{T}$ represents the temperature in the mixing chamber, $T_{G,\,in}$ and $T_{S,\,in}$ are the temperatures of the inflowing gases, $c_{p,G}$ and $c_{p,S}$ are the specific heat capacities, which are assumed to

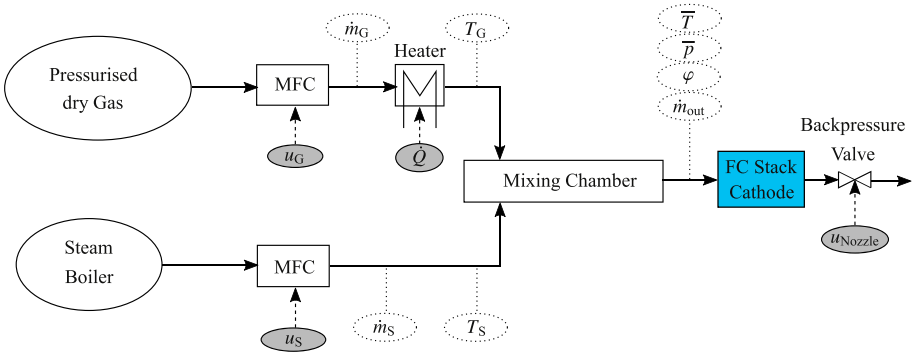

Fig. 2 – Block diagram of testbench for cathode channel.

be constant over the whole operating range, and r_0 is the latent heat of steam.

To obtain an expression for the specific internal energy, we insert Eq. (7) into Eq. (6) and obtain the equations given by Eq. (8).

$$R = c_p - c_v, \quad h = u + pv, \quad RT = pv \tag{7}$$

where R represents the gas constant, c_v the specific heat capacity and v the specific volume.

$$\overline{u}_G = c_{v,G}\overline{T}, \quad \overline{u}_S = c_{v,S}\overline{T} + r_0 \tag{8}$$

By inserting Eq. (6) and Eq. (8) into Eq. (4) and applying the time derivative we obtain the equation

$$\begin{aligned}\frac{d}{dt}\overline{T} = \frac{1}{\overline{m}_G c_{v,G} + \overline{m}_S c_{v,S}} \cdot \Big(& \dot{m}_{G,\,in} c_{p,G} T_{G,\,in} + \dot{m}_{S,\,in}\left(c_{p,S} T_{S,\,in} + r_0\right) \\ & - \frac{1}{\overline{m}} \dot{m}_{out}\left(\overline{m}_G c_{p,G}\overline{T} + \overline{m}_S\left(c_{p,S}\overline{T} + r_0\right)\right) - \frac{d}{dt}\overline{m}_G c_{v,G}\overline{T} \\ & - \frac{d}{dt}\overline{m}_S\left(c_{v,S}\overline{T} + r_0\right)\Big),\end{aligned} \tag{9}$$

which describes the temperature dynamics of our system.

The pressure $\overline{p}$ at the inlet of the fuel cell stack is calculated by using the ideal gas law given in Eq. (10), with R_G and R_S being the gas constants of gas and steam. The volume V of the system enters through this equation. It has an effect on the pressure dynamics of the system and is treated as a parameter. The volume not only represents the volume of the mixing chamber but also the volume of the other piping, which have an effect on the dynamics.

$$\overline{p}V = \left(\overline{m}_G R_G + \overline{m}_S R_S\right)\overline{T} \tag{10}$$

These equations describe the thermodynamics of the system. One important quantity in these equations is the outflowing mass stream $\dot{m}_{out}$, which is highly dependent on the backpressure valve. The relative humidity φ is given by Eq. (11).

$$\varphi = \frac{X}{\frac{R_G}{R_S} + X} \cdot \frac{\overline{p}}{p_W^s(\overline{T})}, \quad X = \frac{\overline{m}_S}{\overline{m}_G} \tag{11}$$

where X represents the vapour content in the gas, and $p_W^s(\overline{T})$ is the saturation partial pressure given by Magnus' formula in Eq. (12).

$$p_W^s(\overline{T}) = p_m \cdot e^{\frac{C_1 \cdot \overline{T}}{C_2 + \overline{T}}} \tag{12}$$

The parameters p_m, C_1 and C_2 for Eq. (12) are taken from Ref. [22].

Pressure valve

To model the mass flow through the backpressure valve, the nonlinear flow equation [23] given in Eq. (13) has been used.

$$\begin{aligned}\dot{m}_{out} &= A\overline{p}\sqrt{\frac{2}{R\overline{T}}} \cdot \psi \\ \psi &= \sqrt{\frac{\kappa}{\kappa - 1}\left[\left(\frac{p_0}{\overline{p}}\right)^{\frac{2}{\kappa}} - \left(\frac{p_0}{\overline{p}}\right)^{\frac{\kappa+1}{\kappa}}\right]}, \quad \kappa = \frac{c_p}{c_v}\end{aligned} \tag{13}$$

The critical pressure is given by

$$\frac{p_0}{\overline{p}} = \left(\frac{2}{\kappa + 1}\right)^{\frac{\kappa}{\kappa - 1}} \tag{14}$$

and the critical flow is given by

$$\psi_{max} = \left(\frac{2}{\kappa + 1}\right)^{\frac{1}{\kappa - 1}} \sqrt{\frac{\kappa}{\kappa + 1}}. \tag{15}$$

In this equation, A represents the opening area of the aperture, R the gas constant and p_0 the ambient pressure. For this equation, we have to take into account that the content of water vapour in the gas mixture changes over the operation range. Therefore, the gas constant R and the specific heat capacities c_p and c_v of the current gas mixture have to be used.

Actuator dynamics of gas conditioning system model

In order to account for the dynamics, which is introduced by the actuators, we incorporate these into the model. There are different approaches how this can be achieved. In our approach, we model the dynamics as first order lag elements with time constants τ_{1-4}. This leads to additional four differential equations given by Eq. (16).

$$\frac{d}{dt}\dot{m}_{G,\,in} = \frac{1}{\tau_1}\left(u_G - \dot{m}_{G,\,in}\right) \tag{16a}$$

$$\frac{d}{dt}T_{G,\,in} = \frac{1}{\tau_2}\frac{1}{c_{p,G}\dot{m}_{G,\,in}}\left(\frac{\dot{Q}}{\dot{m}_{G,\,in}} - c_{p,G}\left(T_{G,\,in} - T_{G,\,0}\right)\right) \tag{16b}$$

$$\frac{d}{dt}\dot{m}_{S,\,in} = \frac{1}{\tau_3}\left(u_S - \dot{m}_{S,\,in}\right) \tag{16c}$$

$$\frac{d}{dt}\dot{A}_{Nozzle} = \frac{1}{\tau_4}\left(u_{Nozzle} - \left(A_{Nozzle} - A_0\right)\right) \tag{16d}$$

Eq. (16a) represents the first order lag element for the gas supply. Eq. (16b) derives from a first order lag element for the energy balance of the heater depicted in Fig. 2 and the assumption that $\frac{d}{dt}\dot{m}_{G,\,in} = 0$ during the heat transfer in the heater. This implies that all the energy provided by the heater is absorbed by increasing the temperature of the current mass flow, but the mass flow itself is not affected by the process. Additionally, a temperature offset $T_{G,\,0}$ has been included. This accounts for the fact that the gas flow can not be cooled below the initial gas temperature provided at the testbed. Eq. (16c) represents the first order lag element for steam supply. Eq. (16d) represents the first order lag element for the backpressure valve with an offset value A_0 for the opening area of the valve.

Coupling of the system

The equations presented in this section are coupled through various relations. This leads to the fact that the input variables can not be associated with the output variables. By changing one input variable, all the output variables are affected in one or another way. This is illustrated in Fig. 3. The figure shows the system response for step changes of the input variables. All the system outputs are affected by each change of the input variables.

In the following, we present a control concept, which will deal with this fact and solves this by decoupling the equations and by creating new input variables, which are directly associated with the output variables.

Model parameters

For the modelling of the system depicted by Fig. 2, some assumptions of the system parameters have been done. These parameters are depending on the system setup and external factors. These parameters are the volume of the piping, which has an effect on the pressure dynamics, the ambient pressure, which enters into the nonlinear flow equation, the constant specific heat capacities of gas and steam and the constant steam temperature. The controller, which will be presented in the following sections, has to be robust against variations of these parameters.

Exact linearisation of MIMO nonlinear system

In the following, we will briefly introduce the concept of exact linearisation and differential flatness. Then we apply these methods to the system model derived in Section PEMFC gas conditioning system to decouple the system. Next, we design a controller for the decoupled system, which achieves both good trajectory tracking and good disturbance rejection.

Exact linearisation of MIMO nonlinear system

Consider a nonlinear MIMO system of the form

$$\begin{aligned} \dot{x} &= f(x) + \sum_{i=1}^{m} g_i(x) u_i \\ y &= h(x) \end{aligned} \tag{17}$$

where x is an n-dimensional state vector, and u and y are m-dimensional input and output vectors.

By applying the time derivative to the output y, we obtain

$$\begin{aligned} \dot{y}_j &= \frac{\partial h_j}{\partial x} f(x) + \sum_{i=1}^{m} \frac{\partial h_j}{\partial x} g_i(x) u_i \\ &= L_f h_j(x) + \sum_{i=1}^{n} L_{g_i} h_j(x) u_i, \quad j = 1, 2, \ldots, m \end{aligned} \tag{18}$$

where L_f and L_g represent the *Lie* derivatives of the scalar output functions h with respect to $f(x)$ and $g(x)$. If $L_{g_i} h_j(x) = 0$ holds, then the input vector u does not have an effect on the corresponding time derivative. Hence we repeat the process of the time derivation. Assuming that in the δ_j-th derivative the input does not vanish, then the input vector u has an effect on this derivative, and the corresponding equation has the form of Eq. (19), and δ_j is called the *relative degree* of the output y_j.

$$y_j^{(\delta_j)} = L_f^{\delta_j} h_j + \sum_{i=1}^{m} \left(L_{g_i} L_f^{\delta_j - 1} h_j \right) u_i \tag{19}$$

The *relative degree* δ_j of the output y_j represents the first time derivative on which the input vector u has an effect. By

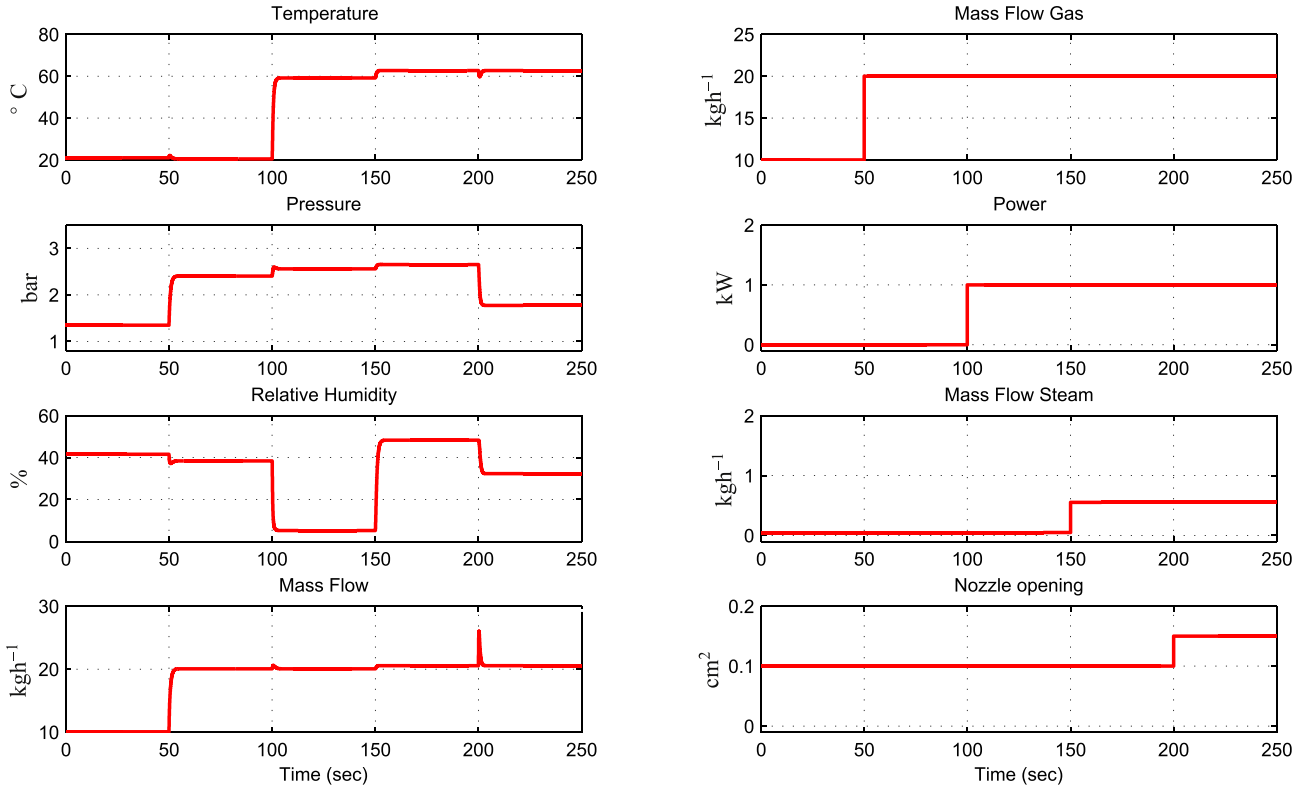

Fig. 3 – Step response of the system model. Plot (a) shows the output trajectories y, and plot (b) shows the corresponding control variables.

applying this to each output y_j, we obtain m equations, which can be written as

$$\begin{bmatrix} y_1^{(\delta_1)} \\ y_2^{(\delta_2)} \\ \vdots \\ y_m^{(\delta_m)} \end{bmatrix} = \underbrace{\begin{bmatrix} L_f^{\delta_1} h_1(x) \\ L_f^{\delta_2} h_2(x) \\ \vdots \\ L_f^{\delta_m} h_m(x) \end{bmatrix}}_{l(x)} + J(x) \begin{bmatrix} u_1 \\ u_2 \\ \vdots \\ u_m \end{bmatrix} \tag{20}$$

where the $(m \times m)$ matrix $J(x)$ is called the decoupling matrix and is defined as

$$J(x) = \begin{bmatrix} L_{g_1} L_f^{\delta_1 - 1} h_1(x) & \dots & L_{g_m} L_f^{\delta_1 - 1} h_1(x) \\ L_{g_1} L_f^{\delta_2 - 1} h_2(x) & \dots & L_{g_m} L_f^{\delta_2 - 1} h_2(x) \\ \vdots & & \vdots \\ L_{g_1} L_f^{\delta_m - 1} h_m(x) & \dots & L_{g_m} L_f^{\delta_m - 1} h_m(x) \end{bmatrix}. \tag{21}$$

By choosing the control law of the form

$$u = \alpha(x) + \beta(x)\, v \tag{22}$$

with

$$\begin{aligned} \alpha(x) &= -J^{-1}(x)\, l(x), \\ \beta(x) &= J^{-1}(x) \end{aligned} \tag{23}$$

one obtains the new *synthetic* input vector v

$$v = \begin{bmatrix} v_1 \\ \vdots \\ v_m \end{bmatrix} = \begin{bmatrix} y_1^{(\delta_1)} \\ \vdots \\ y_m^{(\delta_m)} \end{bmatrix}. \tag{24}$$

From Eq. (24) it is evident that the input–output relation of this system is decoupled and can be represented as a chain of integrators.

If $\sum_{j=1}^{m} \delta_j = dim(x) = n$, the system has so called *full relative degree* and can be transformed into the nonlinear controllable canonical form [24]. The transformation is given by Eq. (25). It utilises the *Lie* derivatives introduced in Eq. (19). The variable z represents the new state of the transformed system.

$$z = \begin{bmatrix} z_1 \\ z_2 \\ \vdots \\ z_{\delta_1} \\ \vdots \\ z_n \end{bmatrix} = T(x) = \begin{bmatrix} h_1(x) \\ L_f h_1(x) \\ \vdots \\ L_f^{\delta_1 - 1} h_1(x) \\ \vdots \\ L_f^{\delta_m - 1} h_m(x) \end{bmatrix} \tag{25}$$

For systems, which do not have *full relative degree*, one has to account for the *internal dynamics* of the system. More on how to deal with *internal dynamics* can be found in Refs. [25] and [26].

The transformation given by Eq. (25) results in the new state space representation, given in Eq. (26), where v represents the new input vector. For this system, linear control methods can be applied.

$$\dot{z} = A_c\, z + B_c\, v \tag{26}$$

The matrices A_c and B_c are given by Eq. (27).

$$A_c = \begin{bmatrix} A_{c,1} & 0 & \dots & 0 \\ 0 & A_{c,2} & \dots & 0 \\ \vdots & \vdots & & \vdots \\ 0 & 0 & \dots & A_{c,m} \end{bmatrix}, \tag{27a}$$

$$B_c = \begin{bmatrix} B_{c,1} & 0 & \dots & 0 \\ 0 & B_{c,2} & \dots & 0 \\ \vdots & \vdots & & \vdots \\ 0 & 0 & \dots & B_{c,m} \end{bmatrix} \tag{27b}$$

where the matrix $A_{c,j}$ is a $(\delta_j \times \delta_j)$ matrix, and $B_{c,j}$ is a $(\delta_j \times 1)$ vector given by Eq. (28).

$$A_{c,j} = \begin{bmatrix} 0 & 1 & 0 & \dots & 0 \\ 0 & 0 & 1 & \dots & 0 \\ \vdots & \vdots & \vdots & & \vdots \\ 0 & 0 & 0 & \dots & 1 \\ 0 & 0 & 0 & \dots & 0 \end{bmatrix}, \quad B_{c,j} = \begin{bmatrix} 0 \\ 0 \\ \vdots \\ 0 \\ 1 \end{bmatrix} \tag{28}$$

Differential flatness

Differential flatness is a property of a class of multivariable nonlinear systems and has first been introduced in Refs. [27] and [28]. A nonlinear system of the form

$$\dot{x} = f(x, u), \quad x(0) = x_0 \tag{29}$$

is said to be differentially flat, if there exists a set of differentially independent variables $y = (y_1, \dots, y_m)$ such that the state variables x and input variables u are functions of these flat outputs and a finite number of their derivatives.

$$y = F(x) \tag{30a}$$

$$x = \Phi(y, \dot{y}, \dots y^{n-1}) \tag{30b}$$

$$u = \Psi(y, \dot{y}, \dots y^{n}) \tag{30c}$$

In that case, y represents the *flat outputs* of the system, and the system is called *differential flat* or *flat system*. The Equation (30) yield that for every given trajectory y, the evolution of the state variables x and input variables u can be calculated without the need to integrate the differential equations.

Exact linearisation of gas conditioning system model

From the equations derived in Section PEMFC gas conditioning system, we formulate the state vector x, the input vector u and output vector y as follows

$$x = \begin{bmatrix} \overline{m}_G \\ \overline{m}_S \\ \overline{T} \\ \dot{m}_{G,\,in} \\ T_{G,\,in} \\ \dot{m}_{S,\,in} \\ A_{Nozzle} \end{bmatrix}, \quad u = \begin{bmatrix} u_G \\ \dot{Q} \\ u_S \\ u_{Nozzle} \end{bmatrix}, \quad y = \begin{bmatrix} \overline{T} \\ \overline{p} \\ \varphi \\ \dot{m}_{out} \end{bmatrix} \tag{31}$$

With this representation, we obtain an equation of the form of Eq. (17). We apply the *Lie* derivatives to the output y and obtain that the first three outputs y_{1-3} have a *relative degree* of two ($\delta_1 = \delta_2 = \delta_3 = 2$), and the last output y_4 has a *relative degree* of one ($\delta_4 = 1$). Due to the complex couplings in the output functions, the *relative degree* of two of these outputs and the dimension of the state vector x, the calculations get

large and are not insightful. For the reason of readability, we do not give the detailed calculations of the *Lie* derivatives.

Since the system has *full relative degree*, we can transform it using the nonlinear transformation introduced in Eq. (25). For our system the transformation takes the form of Eq. (32).

$$z = T(x) = \begin{bmatrix} h_1(x) \\ L_f h_1(x) \\ h_2(x) \\ L_f h_2(x) \\ h_3(x) \\ L_f h_3(x) \\ h_4(x) \end{bmatrix} = \begin{bmatrix} y_1 \\ \dot{y}_1 \\ y_2 \\ \dot{y}_2 \\ y_3 \\ \dot{y}_3 \\ y_4 \end{bmatrix} \tag{32}$$

where, in accordance to Eq. (19), the *Lie* derivatives for the outputs (i = 1,2,3), which have *relative degree* of two ($\delta_i = 2$), yield $L_f h_i(x) = \dot{y}_i$. From this transformation we obtain a system of the form

$$\begin{aligned} \dot{z} &= A_c\, z + B_c\, \beta(x)^{-1}\,(u - \alpha(x)) \\ u &= \alpha(x) + \beta(x)\,\nu \end{aligned} \tag{33}$$

where A_c and B_c are the matrices in controllable canonical form, and ν is the new input variable.

In Fig. 4, the nonlinear transformation of the coupled system given by Eq. (17) into the decoupled system given by Eq. (33) is depicted. Fig. 4b represents a schematic view of the decoupled system as a chain of integrators for each channel. The inputs for the decoupled system are the new input variables ν, which are integrated to obtain the output y. The length of the chain of integrators is equal to the *relative degree* δ_j of the output y_j.

For the decoupling of the system, the knowledge of the state vector x is required, which corresponds to the current operation point of the system. If the states can be measured or observed, they can be fed back into the decoupling matrix. In that case one has to take care of possible feedback disturbances from the system.

Flatness based calculation of the state vector

The system outputs y_{1-4} are *flat* outputs of the system. This can be utilised to minimise the feedback disturbance on the decoupling of the system. Therefore, we apply a flatness-based feedforward calculation of the states x. Instead of using a state vector feedback for the decoupling, we apply the so calculated states x_{FF} in Eq. (33).

The states x_{FF} are calculated offline by solving the set of equations given by Eq. (32). This leads to the functional dependency given in Eq. (30). The so obtained states are then fed into the system.

Trajectory tracking and error dynamics

To achieve both, a good trajectory tracking and good disturbance rejection, we design a Two-Degree-of-Freedom (2DoF) controller for the decoupled system.

We want the output y(t) to track a reference signal $y_{dmd}(t)$. For the decoupled system, the new input variable ν_j represents the input to δ_j chain of integrators. Therefore, the feedforward signal has to be the δ_j-th derivative of the trajectory to be followed by the output y_j. This can be directly seen in Fig. 4b. As controller we choose a $PID^{(\delta-1)}$ control structure, which was introduced in Refs. [29,30]. To design the $PID^{(\delta-1)}$ control structure, we define the tracking error e_j

$$e_j(t) = y_j(t) - y_{dmd,j}(t), \quad j = 1, \ldots, 4 \tag{34}$$

and further the tracking error vector $e_{j,k}$ with $k = 0,\ldots,\delta_j$

$$e_{j,0} = \int_0^t e_j(\tau)\, d\tau, \quad e_{j,1} = e_j, \quad e_{j,2} = \dot{e}_j \tag{35}$$

Combining these, we can write the new input as sum of the feedforward part and the $PID^{(\delta-1)}$ control structure

$$\begin{aligned} \nu_j &= \ddot{y}_{dmd,j} - K_{I,j}\, e_{j,0} - K_{P,j}\, e_{j,1}(t) - K_{D,j}\, e_{j,2}(t), \quad j = 1,2,3 \\ \nu_4 &= \dot{y}_{dmd,4} - K_{I,j}\, e_{4,0} - K_{P,4}\, e_{4,1}(t) \end{aligned} \tag{36}$$

The error dynamics for the first three outputs (j = 1,2,3), which have a relative degree of $\delta_j = 2$, are given by

$$\begin{bmatrix} \dot{e}_{j,0} \\ \dot{e}_{j,1} \\ \dot{e}_{j,2} \end{bmatrix} = \left(\underbrace{\begin{bmatrix} 0 & 1 & 0 \\ 0 & 0 & 1 \\ 0 & 0 & 0 \end{bmatrix}}_{A_{c,j}} - \underbrace{\begin{bmatrix} 0 \\ 0 \\ 1 \end{bmatrix}}_{B_{c,j}} \underbrace{\begin{bmatrix} K_{I,j}, & K_{P,j}, & K_{D,j} \end{bmatrix}}_{K_j} \right) \cdot \begin{bmatrix} e_{j,0} \\ e_{j,1} \\ e_{j,2} \end{bmatrix} \tag{37}$$

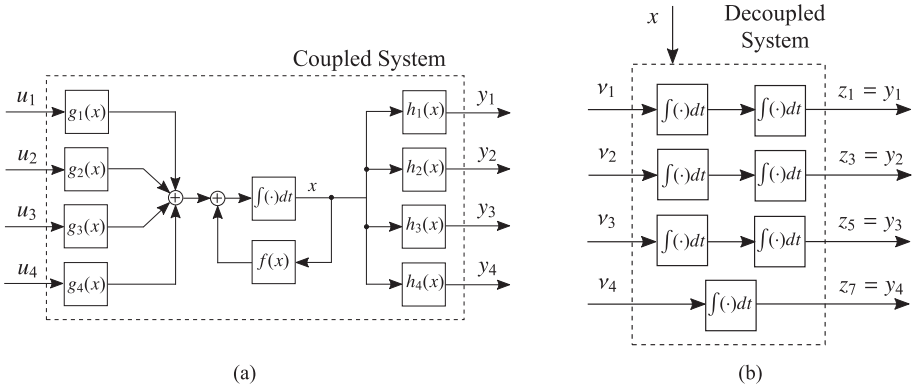

Fig. 4 – Schematic view of the transformation of the coupled system (a) into the decoupled system (b). The decoupled system is represented as chain of integrators with the new input variable ν. The length of the chain of integrators is equal to the *relative degree* δ_j of the output y_j.

and the error dynamics for the fourth output, which has a relative degree of $\delta_4 = 1$, is given by

$$\begin{bmatrix} \dot{e}_{4,0} \\ \dot{e}_{4,1} \end{bmatrix} = \left(\underbrace{\begin{bmatrix} 0 & 1 \\ 0 & 0 \end{bmatrix}}_{A_{c,4}} - \underbrace{\begin{bmatrix} 0 \\ 1 \end{bmatrix}}_{B_{c,4}} \underbrace{\begin{bmatrix} K_{I,4}, & K_{P,4} \end{bmatrix}}_{K_4} \right) \cdot \begin{bmatrix} e_{4,0} \\ e_{4,1} \end{bmatrix} \tag{38}$$

Combining these equations we can rewrite it as

$$\dot{e} = (A_c - B_c K)\, e \tag{39}$$

where e is a (11×1) vector combining Eq. (37), and Eq. (38), A_c is a (11×11) matrix, B_c is a (11×4) matrix, and K is a (4×11) matrix. The vectors and matrices are given in Eq. (40). The asymptotic tracking is achieved by placing the desired poles of $(A_c - B_c K)$ in the left-half plane.

$$A_c = \begin{bmatrix} A_{c,1} & 0 & 0 & 0 \\ 0 & A_{c,2} & 0 & 0 \\ 0 & 0 & A_{c,3} & 0 \\ 0 & 0 & 0 & A_{c,4} \end{bmatrix}, \tag{40a}$$

$$B_c = \begin{bmatrix} B_{c,1} & 0 & 0 & 0 \\ 0 & B_{c,2} & 0 & 0 \\ 0 & 0 & B_{c,3} & 0 \\ 0 & 0 & 0 & B_{c,4} \end{bmatrix}, \tag{40b}$$

$$K = \begin{bmatrix} K_1 & 0 & 0 & 0 \\ 0 & K_2 & 0 & 0 \\ 0 & 0 & K_3 & 0 \\ 0 & 0 & 0 & K_4 \end{bmatrix} \tag{40c}$$

Fig. 5 shows the structure of the system. Σ represents the gas conditioning system, which was modelled by Eq. (1), Eq. (9) and Eq. (16). The decoupling is done by the Σ^{-1} block, which represents Eq. (22). It uses the flatness-based feedforward states x_{FF} to accomplish the decoupling. The channels of the so obtained system are decoupled, and a new input vector ν is introduced. On each channel of this decoupled system, a 2DoF controller is designed to achieve both good trajectory tracking and good disturbance rejection.

For the purpose of clarity we decompose Eq. (39) and write it as

$$\dot{e} = A_c\, e + B_c \left[\beta(x)^{-1} (u - \alpha(x)) - y_{dmd}^{(\delta)} \right] \tag{41a}$$

$$u = \alpha(x) + \beta(x)\, \nu \tag{41b}$$

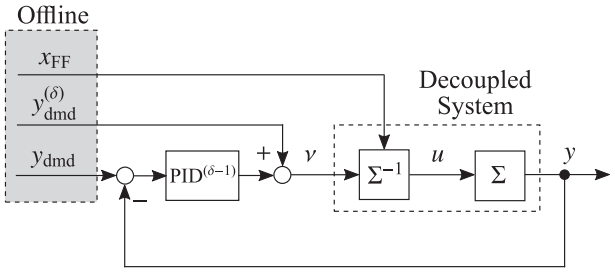

Fig. 5 – Block diagram of Two-Degree-of-Freedom (2DoF) Controller.

$$\nu = y_{dmd}^{(\delta)} - K\, e \tag{41c}$$

In this formulation, the decoupling terms $\alpha(x)$ and $\beta(x)$ appear in the control law. To this representation of the error dynamics we will later refer to discuss the robustness of the system.

Including constraints on the input variables

During operation the following two problems arise in calculating the input vector.

First, the decoupling matrix $J(x)$ is not invertible for all states x. Although this is not the case if the system is in the operating range described in Table 1, for the startup the system has to cross a region, where $J(x)$ does not have full rank. A physical interpretation of the startup is the following: At startup the system pressure $\overline{p}$ is equal to the ambient pressure p_0, and therefore, the backpressure valve has no effect on the outflowing mass flow $\dot{m}_{out}$. Hence, the decoupling matrix $J(x)$ does not have full rank. Therefore, we need an additional condition to invert the decoupling matrix. So we can steer the system into the operating range, where the decoupling matrix $J(x)$ has full rank and the additional condition can be dropped.

Second, constraints on the actuators lead to deviations of the output trajectory. In order to achieve a better trajectory tracking, we want to minimise these deviations.

Both problems can be solved by introducing the following *Lagrange* function

$$\mathcal{L} = \alpha \frac{1}{2} u^T R\, u + \frac{1}{2} \left(y^{(\delta)} - y_{dmd}^{(\delta)} \right)^T Q \left(y^{(\delta)} - y_{dmd}^{(\delta)} \right) + \lambda^T (Mu - \gamma) \tag{42}$$

where R and Q are (4×4) symmetric and positive definite matrices, which are used as weighting matrices, M is a (4×4) identity matrix, and γ is a (4×1) vector of the actuator constraints listed in Table 1.

The first term is active ($\alpha = 1$) if the decoupling matrix is not invertible, otherwise $\alpha = 0$. This minimises additionally the input vector u. This additional condition is responsible for the invertibility of the decoupling matrix $J(x)$ if it does not have full rank.

The second term minimises the deviation of the trajectory curvature. Whereas $(y^{(\delta)} - y_{dmd}^{(\delta)})$ is the equivalent formulation of Eq. (22) for optimisation.

The third term represents the *Lagrange Multiplier* λ for the active constraints. If the constraints are reached by one or more input variables, the constraints are added using the *active-set-method*.

By reformulating Eq. (42) into

$$\mathcal{L} = \frac{1}{2} u^T E\, u + \frac{1}{2} u^T F + \lambda^T (Mu - \gamma) \tag{43}$$

with

$$\begin{aligned} E &= R + J(x)^T Q\, J(x), \\ F &= J(x)^T Q \left(l(x) - y_{dmd}^{(\delta)} \right) \end{aligned} \tag{44}$$

we can write the solution as

$$\begin{aligned} \lambda_{act} &= -\left(M_{act}\, E^{-1} M_{act}^T \right)^{-1} \left(\gamma_{act} + M_{act}\, E^{-1} F \right), \\ u &= -E^{-1} \left(M_{act}^T \lambda_{act} + F \right), \end{aligned} \tag{45}$$

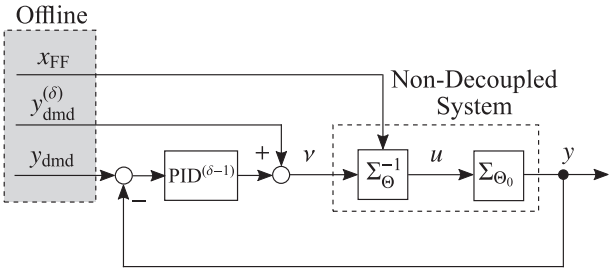

Fig. 6 – System in which the decoupling block Σ^{-1} has a different parameter set Θ than Σ.

Table 2 – Model parameters used for the simulation.

Parameter	Value
Volume	14 137 cm^3
$c_{p,G}$	1.04 kJ kg^{-1} K^{-1}
$c_{p,S}$	1.89 kJ kg^{-1} K^{-1}
T_S	141 °C
p_0	1 bar

where M_{act} and λ_{act} represent the active constraints. The so obtained Eq. (45) replaces Eq. (22) in Σ^{-1} in Fig. 5.

Robustness analysis

In the following, we present a robustness analysis with respect to parameter uncertainties for the derived system. We discuss the robustness of the decoupling of the system in case of deviations of the system parameters and the parameters assumed for the calculation of the decoupling.

System parameters

The method of input–output exact linearisation, which has been applied in Section Exact linearisation of MIMO nonlinear system, relies on the exact cancelation of α and β in Eq. (41a) and the control law Eq. (41b). If this is not the case, a coupling of the output vector y will remain.

To analyse the robustness of the system, we introduce the parameter vector Θ

$$\Theta = \begin{bmatrix} \text{Volume} \\ c_{p,G} \\ c_{p,S} \\ T_S \\ p_0 \end{bmatrix} \tag{46}$$

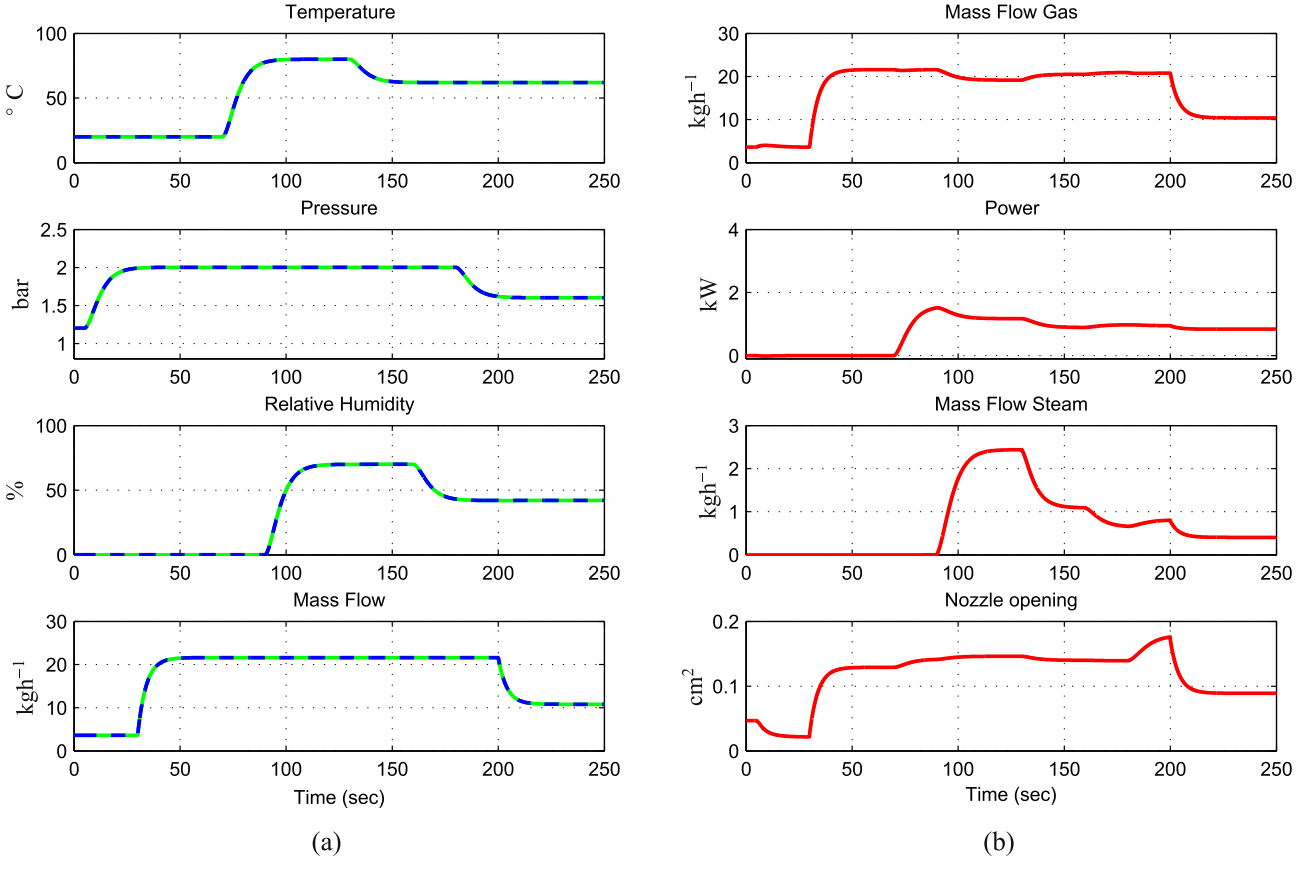

Fig. 7 – Plot (a) shows the achieved output trajectories y (*green full line*) and the desired trajectories y_{dmd} (*blue dashed line*). Plot (b) shows the corresponding control variables. (For interpretation of the references to colour in this figure legend, the reader is referred to the web version of this article.)

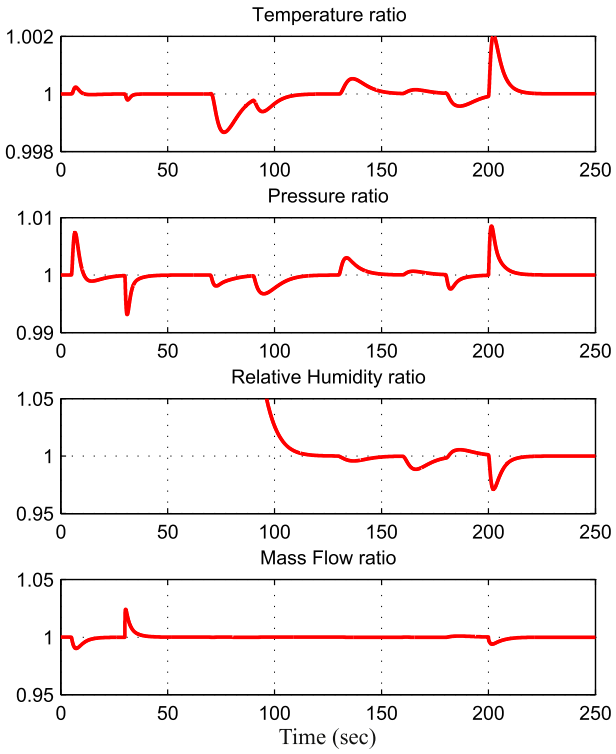

Fig. 8 – Ratio plots of achieved to desired output trajectories for parameter variations.

which contains the parameters discussed in Section PEMFC gas conditioning system. These are the volume of the mixing chamber and the piping, the specific heat capacities, which are assumed to be constant, the steam temperature and the ambient pressure during operation. These parameters have an effect on the dynamics of the system equations derived in Section PEMFC gas conditioning system and enter as well in the calculation of the decoupling derived in Section Exact linearisation of MIMO nonlinear system. Fig. 6 shows the case, where the decoupling block Σ_{Θ}^{-1} and the system Σ_{Θ_0} have a different set of parameters. In that case the system is not fully decoupled.

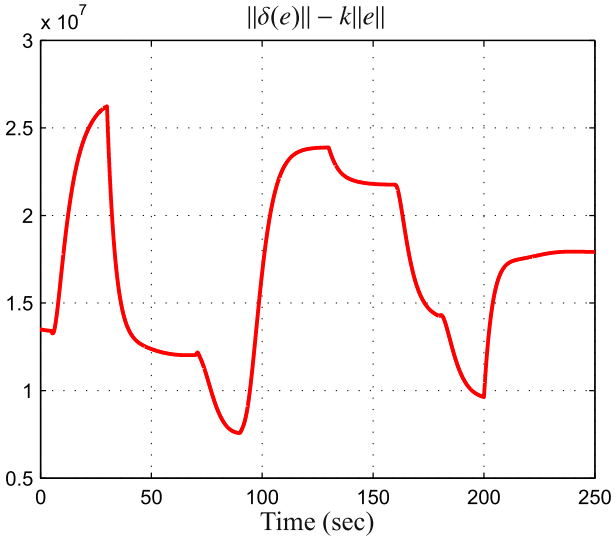

Fig. 9 – Calculated trajectory $||\delta(e)|| - k||e||$ in accordance to Lemma 13.3. For the trajectories one finds an ϵ, which fulfils the Lemma.

Disturbed system

To consider the parameter deviations of the system, we introduce the error of the nominal system Eq. (47a) and the error of the disturbed system Eq. (47b).

$$e_j(t) = y_j(t, \Theta_0) - y_{dmd,j}(t) \tag{47a}$$

$$\hat{e}_j(t) = y_j(t, \Theta) - y_{dmd,j}(t) \tag{47b}$$

where Θ_0 is the unperturbed parameter vector and Θ the perturbed vector. Similar to Eq. (41), the error dynamics of the disturbed system can be written as

$$\begin{aligned} \dot{e} &= A_c\, e + B_c\left[\beta(x)^{-1}(u - \alpha(x)) - y_{dmd}^{(\delta)}\right] \\ u &= \hat{\alpha}(x) + \hat{\beta}(x)\, \nu \\ \nu &= y_{dmd}^{(\delta)} - K\, e \end{aligned} \tag{48}$$

where $\hat{\alpha}$ and $\hat{\beta}$ arise from the disturbed system Σ_{Θ}^{-1}, and α and β arise from the undisturbed system Σ_{Θ_0}. Combining these equations, we obtain

$$\dot{e} = (A_c - B_c\, K)\, e + B_c\, \delta(e) \tag{49}$$

where $\delta(e)$ represents the perturbation of the nominal system, and is given by

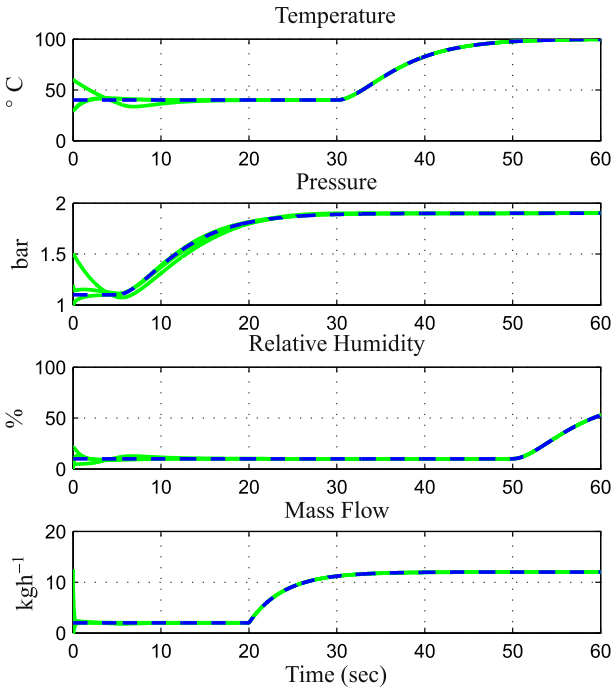

Fig. 10 – Initialisation with different initial conditions. The Plot shows the achieved output trajectories y (*green full line*) and the desired trajectories y_{dmd} (*blue dashed line*). (For interpretation of the references to colour in this figure legend, the reader is referred to the web version of this article.)

Table 3 – Mean squared error for different magnitudes of measurement noise. The magnitude is given as standard deviation of the normal distribution.

Measurement noise	Case 1	Case 2	Case 3
σ_1	0.1 °C	0.5 °C	1 °C
σ_2	0.002 bar	0.01 bar	0.1 bar
σ_3	0.2%	1%	5%
σ_4	0.07 kgh^{-1}	0.1 kgh^{-1}	1 kgh^{-1}
MSE Temperature	$1.6 \cdot 10^{-3}$ °C	$4 \cdot 10^{-3}$ °C	$4.6 \cdot 10^{-2}$ °C
MSE Pressure	$2.8 \cdot 10^{-6}$ bar	$3.8 \cdot 10^{-6}$ bar	$6.4 \cdot 10^{-5}$ bar
MSE Relative Humidity	$6.4 \cdot 10^{-4}$%	$9.5 \cdot 10^{-3}$%	0.3%
MSE Mass Flow	$1.3 \cdot 10^{-3}$ kgh^{-1}	$1.5 \cdot 10^{-3}$ kgh^{-1}	$3.6 \cdot 10^{-2}$ kgh^{-1}

Table 4 – The different initial conditions for the system outputs y_j, which are used in the simulation.

Output	Case 1	Case 2	Case 3
y_1	60 °C	10 °C	30 °C
y_2	1.5 p_0	0.8 p_0	1.2 p_0
y_3	5%	21%	0%
y_4	3 kgh^{-1}	0 kgh^{-1}	21 kgh^{-1}

$$\delta(e) = \beta^{-1}\left[(\widehat{\alpha} - \alpha) + \left(\widehat{\beta} - \beta\right)\left(y_{dmd}^{(\delta)} - K\,e\right) + \widehat{\beta}\,K\,(e - \widehat{e})\right] \quad (50)$$

The perturbation term $\delta(e)$ arises from the incomplete decoupling of the system and affects all four decoupled systems. To study the effect of this perturbation on the system, we apply the following Lemma taken from Ref. [26].

Lemma 13.3 Consider the closed-Loop system (49), where $(A_c - B_cK)$ is Hurwitz.Let $P = P^T > 0$ be the solution of the Lyapunov equation

$$P(A - BK) + (A - BK)^T P = -I$$

and k be a nonnegative constant less than $1/(2||PB||_2)$.

- If $||\delta(e)|| \leq k\,||e||$ for all e, the origin of (49) will be globally exponentially stable.
- If $||\delta(e)|| \leq k\,||e|| + \epsilon$ for all e, the state e will be globally ultimately bounded by ϵc for some c>0.

The proof of this Lemma can be found in [26]. For each trajectory y_{dmd}, we can calculate an upper boundary in accordance to the Lemma. Simulation results for the parameter varied system will be shown in the following section.

Simulation results

In the following, the simulation results for the proposed nonlinear multivariable control strategy are presented. The parameters used for the simulation are listed in Table 2.

Results for the decoupled system

The simulations have been performed with setpoint changes in the operating range defined in Table 1. Whereas the trajectories for the setpoint changes have been calculated in accordance to the *relative degree* of the corresponding output. Fig. 7a shows the comparison of the desired trajectories y_{dmd} (*blue dashed line*) and the achieved output trajectories y (*green full line*) of the system. The plot shows good agreement for all trajectories. The poles of the controllers have been placed as following: For the channels with $\delta = 2$, the poles are at $s_1 = -1$, $s_{2,3} = -8 \pm 1j$, and for the channel with $\delta = 1$, the poles are at $s_{1,2} = -5$. This configuration is robust for a wide range of tested parameter variations. The results for disturbances on the system are shown in Section Simulation results for disturbances on the system.

The corresponding control inputs u are shown in Fig. 7b. The coupling of the system can be seen on the control inputs. For each alteration of the trajectories shown in Fig. 7a, all control inputs have to be altered in order to achieve the decoupling and hence the desired output trajectory y.

The limiting factors for the trajectory slopes are the actuator dynamics, which we modelled by first order lag elements. In order to achieve a fast response of the system, the actuators have to be able to follow the rapid change of the control input.

Simulation results for disturbances on the system

Fig. 8 shows simulation results for the parameter varied system. The plot shows the ratio of achieved to desired output trajectories for a parameter varied system. For the simulation the entries of the parameter vector Θ have been varied by the following values: Volume −50%, $c_{p,G}$ + 50%, $c_{p,S}$ − 50%, T_S + 50%, p_0 + 50%. Therefore, the system is not fully decoupled, and the $PID^{(\delta-1)}$ controller has to correct the trajectories. For the simulations the controller configuration introduced in Section Results for the decoupled system are used, which is robust for a wide range of tested parameter variations.

The plot shows that small deviations from the desired trajectory appear, and the controller has to correct the trajectories. The largest deviation is around 1 – 2%, which is sufficiently small. The simulations also show that the flatness-based feedforward calculation of the states x stabilises the decoupling of the system, and no feedback disturbances affect the decoupling matrix.

Additionally, we investigate the stability of the system for parameter uncertainties as introduced in Section Robustness analysis. Therefore, we calculate the error $\delta(e)$ in Eq. (49). Fig 9 shows the calculated value of $||\delta(e)|| - k\,||e||$ in accordance to the Lemma presented in Section Robustness analysis. The plot illustrates that for the trajectories y_j we can find an ϵ, which fulfils the Lemma stated in Section Robustness analysis.

Therefore, we conclude that the system along this trajectories is robust against this perturbation of parameters.

The effect of the initial conditions on the system are investigated by choosing different initial conditions and test for the convergence of the system. In Fig. 10 three different initial conditions for the system outputs y_j are chosen. The values for the system outputs are given in Table 4. Due to the flatness of the system the state vector x_0 can be calculated from the system outputs. The simulation shows that for all three initial conditions the trajectories y_j converge to the desired trajectories y_{dmd}.

The effect of measurement noise on the performance of the controller is investigated by applying a normal distributed noise on the output variables y_j. The standard deviations for the noise are given in Table 3. The deviation is evaluated as the mean squared error of the output variables y_j and the trajectories y_{dmd}. Due to the feedforward part of the controller the noise does not affect the decoupling and the controller shows stable performance for the investigated noise levels.

Conclusion

In this paper we present a control concept for a highly dynamic testing environment for PEMFC stacks, which controls the inlet gas temperature, stack pressure, relative humidity and gas mass flow.

Based on a presented hardware concept, we derive a system model, which presents a nonlinear control problem with multiple inputs and multiple outputs. In order to achieve a better dynamic response of the system, we incorporate the actuator dynamics of the gas conditioning system as first order lag elements.

To this coupled set of equations we apply the method of exact input–output linearisation and decouple the system. In order to achieve a robust decoupling, we take advantage of the differential flatness of the system. The constraints on the actuators are included by formulating the control law as an optimisation problem. For the resulting decoupled system, we design a 2DoF controller with a feedforward part and a PID like control structure. The performed simulations show that the presented decoupling of the system and the designed controller are able to achieve a good trajectory tracking.

The robustness of the system against parameter uncertainties is tested by considering the error of the decoupling as perturbation of the nominal system. To this disturbed system, we apply Lyapunov's stability theory and show that the concept is robust for the tested parameter uncertainties.

Additionally, we investigate the presented control concept for the effect of different initial conditions of the system and the impact of measurement noise on the system.

Acknowledgement

This work was supported by the Austrian Research Promotion Agency (FFG, No. 840395) in cooperation with AVL List GmbH and the Hydrogen Center Austria (HyCentA).

REFERENCES

[1] European Parliament, Regulation (eu) no 333/2014 of the european parliament and of the council of 11 march 2014 amending regulation (ec) no 443/2009 to define the modalities for reaching the 2020 target to reduce CO_2 emissions from new passenger cars, Off J European Union (Downloaded 18/11/2015).

[2] Zhang J, Zhang H, Wu J, ZhangJiujun. PEM fuel cell testing and diagnosis. Amsterdam: Elsevier; 2013. http://dx.doi.org/10.1016/B978-0-444-53688-4.00008-5.

[3] Taniguchi A, Akita T, Yasuda K, Miyazaki Y. Analysis of electrocatalyst degradation in PEMFC caused by cell reversal during fuel starvation. J Power Sources 2004;130(1):42–9.

[4] Taniguchi A, Akita T, Yasuda K, Miyazaki Y. Analysis of degradation in PEMFC caused by cell reversal during air starvation. Int J Hydrogen Energy 2008;33(9):2323–9.

[5] Yousfi-Steiner N, Moçotéguy P, Candusso D, Hissel D, Hernandez A, Aslanides A. A review on PEM voltage degradation associated with water management: impacts, influent factors and characterization. J Power Sources 2008;183(1):260–74. http://dx.doi.org/10.1016/j.jpowsour.2008.04.037.

[6] Damour C, Benne M, Grondin-Perez B, Chabriat J-P, Pollet BG. A novel non-linear model-based control strategy to improve PEMFC water management the flatness-based approach. Int J Hydrogen Energy 2015;40(5):2371–6. http://dx.doi.org/10.1016/j.ijhydene.2014.12.052.

[7] Haddad A, Bouyekhf R, El Moudni A. Dynamic modeling and water management in proton exchange membrane fuel cell. Int J Hydrogen Energy 2008;33(21):6239–52. http://dx.doi.org/10.1016/j.ijhydene.2008.06.014.

[8] Matraji I, Laghrouche S, Wack M. Pressure control in a PEM fuel cell via second order sliding mode. Int J Hydrogen Energy 2012;37(21):16104–16. advances in Hydrogen Production (Selected papers from ICH2P-2011), http://dx.doi.org/10.1016/j.ijhydene.2012.08.007.

[9] Matraji I, Ahmed FS, Laghrouche S, Wack M. Comparison of robust and adaptive second order sliding mode control in PEMFC air-feed systems. Int J Hydrogen Energy 2015;40(30):9491–504. http://dx.doi.org/10.1016/j.ijhydene.2015.05.090.

[10] Pukrushpan J, Stefanopoulou A, Peng H. Modeling and control for PEM fuel cell stack system. In: American Control Conference, 2002. Proceedings of the 2002, vol. 4; 2002. p. 3117–22. http://dx.doi.org/10.1109/ACC.2002.1025268.

[11] Pukrushpan J, Peng H, Stefanopoulou AG. Control-oriented modeling and analysis for automotive fuel cell systems. J Dyn Syst Meas Control 2004;126(1):14–25.

[12] Rodatz P, Paganelli G, Guzzella L. Optimizing air supply control of a PEM fuel cell system. In: American Control Conference, 2003. Proceedings of the 2003, vol. 3. IEEE; 2003. p. 2043–8.

[13] Na W, Gou B, Diong B. Nonlinear control of PEM fuel cells by exact linearization. In: Industry Applications Conference, 2005. Fourtieth IAS Annual Meeting. Conference Record of the 2005, Vol. 4; 2005. p. 2937–43. http://dx.doi.org/10.1109/IAS.2005.1518877.

[14] Na W, Gou B. Feedback-linearization-based nonlinear control for PEM fuel cells. IEEE Trans Energy Convers 2008;23(1):179–90.

[15] Li Q, Chen W, Wang Y, Jia J, Han M. Nonlinear robust control of proton exchange membrane fuel cell by state feedback exact linearization. J Power Sources 2009;194(1):338–48. XIth Polish Conference on Fast Ionic Conductors 2008, http://dx.doi.org/10.1016/j.jpowsour.2009.04.077.

[16] Danzer MA, Wilhelm J, Aschemann H, Hofer EP. Model-based control of cathode pressure and oxygen excess ratio of a PEM fuel cell system. J Power Sources 2008;176(2):515–22.
[17] Ou K, Wang Y-X, Li Z-Z, Shen Y-D, Xuan D-J. Feedforward fuzzy-PID control for air flow regulation of PEM fuel cell system. Int J Hydrogen Energy 2015;40(35):11686–95.
[18] Kim Y, Kang S. Time delay control for fuel cells with bidirectional DC/DC converter and battery. Int J Hydrogen Energy 2010;35(16):8792–803. http://dx.doi.org/10.1016/j.ijhydene.2010.05.022.
[19] Gruber J, Doll M, Bordons C. Design and experimental validation of a constrained MPC for the air feed of a fuel cell. Control Eng Pract 2009;17(8):874–85. http://dx.doi.org/10.1016/j.conengprac.2009.02.006.
[20] Rehrl J, Horn M. Temperature control for HVAC systems based on exact linearization and model predictive control. In: Control Applications (CCA), 2011 IEEE International Conference on. IEEE; 2011. p. 1119–24.
[21] Thosar A, Patra A, Bhattacharyya S. Feedback linearization based control of a variable air volume air conditioning system for cooling applications. ISA Trans 2008;47(3):339–49.
[22] Plant RS, Yano J-I. Parameterization of atmospheric convection, vol. 1. Imperial College Press; 2015.
[23] Elger D, Williams B, Crowe C, Roberson J. Engineering fluid mechanics, vol. 10. Wiley; 2012.
[24] Isidori A. Nonlinear control systems. 3rd ed. Secaucus, NJ, USA: Springer-Verlag New York, Inc.; 1995.
[25] Slotine J-J, Li W. Applied nonlinear control. Prentice Hall; 1991.
[26] Khalil HK. Nonlinear systems, vol. 3. Prentice Hall; 2002.
[27] Fliess M, Lévine J, Martin P, Rouchon P. Flatness and defect of non-linear systems: introductory theory and examples. Int J Control 1995;61(6):1327–61. http://dx.doi.org/10.1080/00207179508921959. http://dx.doi.org/10.1080/00207179508921959.
[28] Fliess M, Lévine J, Martin P, Rouchon P. A lie-backlund approach to equivalence and flatness of nonlinear systems. IEEE Trans Automatic Control 1999;44(5):922–37.
[29] Hagenmeyer V, Delaleau E. Exact feedforward linearization based on differential flatness. Int J Control 2003;76(6):537–56.
[30] Hagenmeyer V, Delaleau E. Robustness analysis of exact feedforward linearization based on differential flatness. Automatica 2003;39(11):1941–6.